Ab Initio and Density Functional Calculations of the Energies of the Singlet and Triplet Valence Excited States of Pyrazine

Peter Weber and Jeffrey R. Reimers*

School of Chemistry, University of Sydney, NSW 2006 Australia

Received: April 28, 1999; In Final Form: September 16, 1999

A total of 33 ab initio or density functional schemes are applied to evaluate the vertical excitation energies of each of six pyrazine triplet excited states while 22 schemes are applied for each of eight singlet excited states; recent EOM-CCSD(T) results for the singlet states are also considered. The highest quality results are obtained using CASPT2, B3LYP, and EOM-CCSD(T) methodologies. Time-dependent density functional methods are found to produce excitation energies for triplet states in excellent agreement with those evaluated directly. For singlet states, the state-average method, which is commonly used to treat spin contamination, is found to give poor results compared to those given by time-dependent density functional theory. While the notionally most reliable calculations support the (contentious) assignment of $^3B_{1u}$ and $^3B_{2u}$ as given by Walker and Palmer, the errors associated with the methods are too large to provide an authoritative assignment. Reorganization energy calculations indicate that ^3A_u is very broad and has been incorrectly assigned; they also suggest that this state could be responsible for the observed chaos in the $S_0 \rightarrow T_1$ absorption spectrum of pyrazine crystal as well as the observed high vibrational relaxation efficiency of T_1.

I. Introduction

The electronic structures of the azabenzenes have been studied extensively using a range of experimental techniques,[1] and, as a result, these molecules have often been used for the verification of new computational schemes.[2−13] For many, the identities of a variety of low-lying excited states are now known.[1,14] Typically, however, insufficient purely experimental evidence can be gleaned in order to produce a complete analysis, either because some electronic states are "dark" to all available techniques, or because the data suggest a range of possible interpretations. Ab initio computational methods for determining the excited states of small molecules with on the order of 6 to 10 heavy atoms have advanced significantly in recent years, but absolute error bars tend to be within the range of 0.2−0.5 eV. As excited-state energy differences are often smaller than this, these computational methods often cannot reproduce important fine details. However, by combining available experimental and computational information, a reasonable description of the low-lying excited states can regularly be obtained. For pyrazine, 6−8 excited states have been observed experimentally in the singlet and triplet manifolds. Assignments of these states have been suggested[6,15,16] and questioned;[17] while some assignments are clear from experimental data, others are based on computational results. Also, it is clear from computation that some low-lying singlet and triplet states remain to be observed.

We review the assignments of the singlet and triplet states of pyrazine by examining the reliability of the computational methods used in making the assignments. In principle, ab initio calculations can provide results of very high accuracy, sufficient to answer all unresolved questions. However, the computational resources required increase very rapidly with both the level of theory and increasing molecular size. One of the best available ab initio methods, CASPT2 (see later), for example, is quite feasible for single-point energy calculations on pyrazine and it has been applied for porphyrin,[18] but applications to larger systems are unlikely in the near future. Other newly developing methods such as EOM-CCSD(T)[13] are also expensive.

In recent years density functional techniques have had a dramatic impact on ground-state computations as they are more readily applicable to large systems than are ab initio Hartree−Fock self-consistent field (SCF) based calculations. Progress on the application of these techniques to excited states has been much slower, however, principally because of the absence of a rigorous general formalism. A variety of approaches have been introduced, with reasonable success, and in this work we investigate three different density functional methods through calculations for the triplet and singlet excited states of pyrazine, comparing the results to those obtained from a variety of (typically more computationally intensive) ab initio approaches as well as the computationally very efficient semiempirical CNDO/S-CI[19,20] approach. All methods used are described in detail in section II; in total, 22 schemes are used to evaluate singlet vertical excitation energies while 33 are used for the triplet states. Results obtained using other[6,13,16] high-level computational methods are also assimilated.

After examining the reliability of the quantum chemical techniques, we review the assignments of the experimentally observed electronic states. For the singlet states, this assignment appears firm, the most significant issue relating to the location of the unobserved ^1A_u state. For the triplet states, only $^3B_{3u}$ and $^3B_{2g}$ have firm assignments; four additional states have been observed but their assignment is based largely on matching the observed energies to those calculated, and the first complete assignment, that of Walker and Palmer,[16] has been debated by Fischer.[17]

Experimentally, assignment of an observed transition often requires the analysis of vibrational fine structure. Computation can assist this through the evaluation of adiabatic potential energy surfaces and through the analysis of nonadiabatic (or

* Corresponding author.

10.1021/jp991403s CCC: $18.00
Published on Web 11/03/1999

vibronic) coupling.[14] Complete excited-state vibrational analyses are very rare, and, in a subsequent paper, we perform vibrational analyses for a variety of excited states of pyrazine and compare the results to the available experimental data.[21] Such analyses provide detailed high-resolution information but are computationally very expensive. However, important low-resolution information can be obtained by simply optimizing the geometry of the excited state. During this process the energy falls from the vertical excitation energy, the average absorption frequency, to (excluding zero-point energy effects) that of the 0−0 transition; this is called the *reorganization energy* λ of the excited state. For pyrazine and most molecules, the reorganization energy is approximately that from the onset to the maximum of the absorption band, and is readily determined from low resolution spectra. If both absorption and emission spectra are observed experimentally, as is[22] the case for pyrazine S_1, the reorganization energy is given as half of the shift between the band maxima. Here, we show how this information can be used to verify state assignments.

II. Computational Methods

A variety of computational methods are employed, as described below. Unless otherwise stated, all calculations are performed using the cc-pVDZ basis set.[23] All vertical excitation energies are evaluated at the optimized B3LYP/cc-pVDZ geometry of the ground-state S_0; for this state, the calculated CN, CC, and CH bond lengths of 1.339, 1.399, and 1.095 Å, respectively, which differ by at most 0.002 Å from the experimental values,[16] while the heavy-atom bond angles differ by only a fraction of a degree. This and other geometric data are given later in Table 7. As noted previously,[16] the calculated ground-state geometry of pyrazine is reasonably insensitive to the computational method used. Also, cc-pVDZ appears as an optimal basis set[16,24] for valence excited states; all of the states considered here are basically of valence type, but we do perform some calculations with the augmented basis set aug-cc-pVDZ[25] to check for partial Rydberg character.

(a) SVWN, B3P86, and B3LYP Methods (Triplet States Only). The local-density approximation SVWN,[26,27] the nonlocal B3P86[28] functional, and the hybrid B3LYP functional[29] are directly implemented for triplet excited states using the Gunnarsson−Lundqvist theorem.[30] This theorem shows that the Kohn−Sham method may rigorously be applied to evaluate the energy of the lowest triplet state belonging to each irreducible representation of the molecular point-group symmetry. We implement this using *Gaussian-94*[31] (the results are named SVWN, B3P86, and B3LYP) as well as the Amsterdam density functional package[32] (results named SVWN-ADF and B3P86-ADF) using the polarized double-ζ quality ADF #III basis set. By setting the orbital occupancy to that corresponding to some high-lying triplet excited state, it is also possible to find additional, unstable, self-consistent solutions to the Kohn−Sham equations. This approach is not reliable as the electron density may spontaneously collapse to that of a lower-energy state, but nevertheless we apply it and do obtain some useful results.

(b) SVWN-AVE, B3P86-AVE, and B3LYP-AVE Methods (Singlet States Only). Technically, the above application of the Gunnarsson−Lundqvist theorem[30] requires the use of spin-unrestricted orbitals; one simply sets the occupancy of the alpha and beta orbitals to reflect the desired electronic state, selecting triplet spin. While this theorem does not apply to singlet excited states, it is instructive to consider what happens when one repeats this procedure selecting singlet spin. An analogous problem arises in Hartree−Fock based theories and is illustrated in Figure 1 in which, within a two-orbital subspace, we show (A) the electronic ground state, (B) a component of the triplet excited state, and (C) and (D) two degenerate components relevant to the singlet singly excited state. Wave function (B) is an eigenstate of electron spin and it does not interact with the other two components of the triplet state. Wave functions (C) and (D) are neither purely singlet nor purely triplet, however, and an interaction occurs between them; this is called *spin contamination*, their symmetric linear combination forming a singlet wave function while the antisymmetric linear combination forms another component of the triplet wave function.

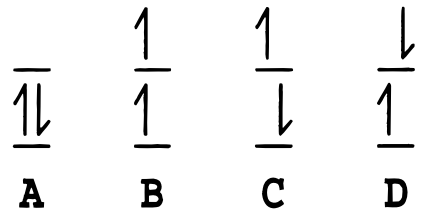

Figure 1. Possible wave functions involving two electrons in two orbitals: (A) ground-state singlet, (B) a component of the triplet excited state, (C) and (D) equivalent spin-contaminated wave functions that are neither singlet nor triplet.

Spin contamination can be readily treated using multiconfiguration SCF (MCSCF) approaches, or, as the spin-adapted wave functions can be specified analytically,[33,34] more simply through restricted open-shell Hartree−Fock (ROHF) theory. Unfortunately, these approaches do not rigorously appear as part of density functional schemes as the orbitals are used simply to represent the density and are not used to form wave functions. Heuristically, one can proceed by assuming that the orbitals can be used to form wave functions and hence eliminate the spin contamination.[35−37] In common use (see e.g., refs 34, 35, 38−40), however, is a less sophisticated approach. It is based on the fact that, for a given occupied orbital set, the SCF energy of the spin-contaminated wave function is the *average* of the energies of the singlet and triplet wave functions. In a ROHF calculation, the program makes this correction (eliminating the spin contamination) at each step in the SCF procedure and the result is an appropriate singlet wave function and energy. As is commonly applied to density-functional methods, the density and energy of the triplet and spin-contaminated states are individually optimized, and, heuristically, the energy of the singlet state is approximated assuming that the energy of the spin-contaminated state remains the average of the singlet and triplet energies, i.e.,

$$E(\text{singlet}) \approx 2E(\text{spin contamined}) - E(\text{triplet}) \qquad (1)$$

This method is unsatisfactory in that no density is produced and analytical gradients are not readily obtained. Also, numerically less satisfactory results have been obtained compared to explicit (heuristic) embedding of the spin projection within the DFT calculation.[35,37] Nevertheless, this method is readily applicable using existing computer software and it has proven successful in a variety of applications.[39,40] Other implementations of density-functional theory to excited states have been suggested (see, e.g. refs 41−54) which we do not consider. In particular, the popular Kohn−Sham eigenvalue method,[49,50,55] in which excitation energies are approximated by Kohn−Sham eigenvalue differences, cannot differentiate between singlet and triplet states and is clearly inappropriate in this application.

(c) SVWN-TDDFT, B3P86-TDDFT, and B3LYP-TDDFT Methods. We apply time-dependent density-functional (TDDFT) to determine the vertical excitation energies of both singlet

TABLE 1: Description of the Orbital Spaces Used in CASSCF and Related Calculations

	doubly occupied								active space							
calculation[a] (*n*,*m*)	a_g	b_{3u}	b_{2u}	b_{1g}	b_{1u}	b_{2g}	b_{3g}	a_u	a_g	b_{3u}	b_{2u}	b_{1g}	b_{1u}	b_{2g}	b_{3g}	a_u
(10,8)	5	0	4	0	4	0	3	0	1	2	0	1	1	2	0	1
(12,11)	5	0	4	0	4	0	2	0	1	2	0	1	2	2	2	1
(12,14)	5	0	4	0	4	0	2	0	3	2	1	1	2	2	2	1
Roos (10,10)	5	0	4	0	4	0	3	0	2	2	0	1	2	2	0	1
Roos (6,12)	6	0	4	0	5	0	3	0	0	4	0	2	0	4	0	2

[a] *n* is the number of active electrons and *m* is the number of orbitals through which they are distributed. The (10,10) active space was used by Roos et al.[6] for (n,π*) excitations while the (6,12) active space was used for (π,π*) excitations.

and triplet excited states. In this approach, the response of a density functional to an applied time-dependent electric field is examined, and we apply the method of Bauernschmitt and Ahlrichs[12,56−59] as implemented in TURBOMOLE.[60] This is a rigorous scheme that estimates the poles in the frequency-dependent molecular polarizability (i.e., the electronic transition energies) through an adiabatic approximation which replaces the full time-dependent exchange-correlation functional with one which is local in time. It has been successfully applied[12] to calculate the singlet excited-state energies of N_2, CH_2O, C_2H_4, pyridine, and free-base porphyrin. However, from these previous calculations on singlet states, it is unclear as to whether calculated discrepancies with experiment should be attributed to shortcomings in the density functional or to breakdown of the adiabatic approximation used in the TDDFT. Here, through comparison of results obtained for triplet states using the method of section (a), the effects of the adiabatic approximation are directly exposed.

(d) UHF, PUHF, UMP2, and PUMP2 Methods (Triplet States Only). These singlet-determinant SCF-based schemes are applied to the triplet excited states using *Gaussian-94*[31] in direct analogy to the direct density functional methods. Calculations are performed using spin-unrestricted Hartree−Fock theory (UHF) and its triplet spin-projected variant (PUHF). Also, dynamic electron correlation is taken into account using spin-unrestricted Møller−Plesset perturbation theory (UMP2) and its spin-projected variant (PUMP2).

(e) CIS Method. This involves the evaluation of singlet and triplet excited-state energies through the solution of the configuration−interaction problem in which all possible single excitations from the ground-state reference determinant are considered.[61] It is implemented using *Gaussian-94*.[31]

(f) CASSCF, CASPT2D, CASPT2, CASPT3, MRCI, and MRCI+Q Methods. All of these methods involve the use of multi-determinant wave functions. The complete active space self-consistent field (CASSCF) geometry optimizations are performed using MOLCAS.[62] CASPT2 involves the application of second-order Møller−Plesset perturbation theory[63] to the CASSCF wave function, and calculations are performed using MOLCAS[62] and sometimes MOLPRO;[64] MOLPRO is also used for calculations to third-order perturbation theory, CASPT3,[65] while results for the diagonal approximation to CASPT2, CASPT2D, are taken from Fülscher, Andersson, and Roos.[6] Contracted multireference configuration interaction[66,67] (MRCI) calculations, possibly including the Davidson[68] correction for quadruple excitations (MRCI+Q), are performed using MOLPRO.[64]

The quality of the results obtained from all of these methods is related to the size of the active space employed. We use the notation (*n*,*m*) to indicate that the active space is obtained by forming all spin-allowed excitations involving *n* electrons distributed through *m* orbitals. The active spaces used are detailed in Table 1 and are of two different types: either single active spaces designed to handle all of the states of interest, or dual active spaces, one for (n,π*) transitions and a different one for (π,π*) transitions. Of the general active spaces, the smallest, (10,8), comprises the six valence π orbitals and the two lone-pair orbitals and is the smallest possible active space of this type. It is appropriate only for structures of D_{2h} symmetry, however; the largest active space which we use is (12,14) which is in fact the smallest active space which is appropriate for all states of interest at arbitrary geometries. Active spaces with these properties are chosen as our interests lie not only in the calculation of vertical excitation energies but also in the nature of the potential energy surfaces,[21] which, because of vibronic coupling, are very sensitive to the properties of all nearby states. The dual active spaces which we use are those designed by Roos et al.[6,69] for the purpose of evaluating the most stable CASPT2 vertical excitation energies. They have the advantage of the direct inclusion of some strongly coupled Rydberg states within the active space, hence stabilizing perturbation theory approaches such as CASPT2. While no Rydberg states are included in the single active spaces, even the (10,8) active space includes a large number of more weakly coupled states which are not included in the (6,12) (π,π*) space of Roos et al., however, and we find that the contribution to the CASPT2 wave function from the reference CASSCF configuration is typically 1−2% less for the Rydberg-containing active space.

No state averaging is used for the lowest energy state of each irreducible representation, but for second-lowest states, the target state is weighted 95% while the lower-energy state is weighted 5%. Issues concerning continuity of potential energy surfaces obtained using these methods, and active-space size and state-averaging in respect thereto, are discussed in detail elsewhere.[21]

(g) CNDO/S-CI Method. Developed some 30 years ago,[19,20] the complete neglect of differential overlap with singles configuration interaction (CNDO/S-CI) semiempirical scheme has been widely applied to determine properties of molecular excited states. It remains the most economic method for large molecules, with recent applications including those to porphyrin oligomers.[70,71] All calculations are performed using our generalized INDO-MRCI program.[72]

III. Evaluation of Vertically Excited State Energies

The location of at least the six lowest triplet states for pyrazine has been determined by a variety of experimental and theoretical techniques, culminating in the work of Walker and Palmer.[16] Of these, the assignment of two states $T_1(^3B_{3u})$ and $T_5(^3B_{2g})$ is clear while those for the four states observed at 4.0, 4.2, 4.4−4.6, and 5.5−5.7 eV are based only on the results of multi-reference doubles configuration−interaction (MRDCI) calculations. These calculations[16] used 27 reference determinants and a double-ζ basis set. Our computed energies for all six states, along with the assignments of Walker and Palmer[16] and the results of their MRDCI calculations are given in Table 2; they are shown graphically in Figure 2. A large number of states

TABLE 2: Triplet Vertical Transition Energies, in eV, of Pyrazine at the B3LYP/cc-pVDZ Ground State Geometry and the RMS Difference from the Assignments of the Observed Energies by Walker and Palmer[16]

									RMS error	
method	basis[a]	log t^b	$T_1\ ^3B_{3u}$	$T_2\ ^3B_{1u}$	$T_3\ ^3A_u$	$T_4\ ^3B_{2u}$	$T_5\ ^3B_{2g}$	$T_6\ ^3B_{1u}$	$T_1 \rightarrow T_6$	T_1, T_5
observed[16]			3.42[c]	4.0[d]	4.2[d]	4.5 ± 0.1[d]	4.59	5.7 ± 0.2[d]		
CNDO/S-CI		−1.0 i	3.52	2.66	5.42	3.20	4.88	4.23	1.10	0.22
PUHF	1	3.2 g	3.87	2.52	5.92	3.59	5.61	3.96	1.31	0.79
PUMP2	1	3.7 g	3.36	5.00	4.57	4.99	4.96	5.68	0.50	0.27
CIS	1	2.5 g	4.09	3.47	6.70	4.26	5.46	5.24	1.16	0.78
CIS	3	3.6 g	4.07	3.45	6.66	4.00	5.42	5.16	1.16	0.75
SVWN	1	2.9 g	3.00	4.69	4.02	4.50	4.63	5.37	0.36	0.30
SVWN-TDDFT	1	2.9 t	2.86	4.54	3.70	4.29	4.36	5.31	0.43	0.43
SVWN-ADF	2	2.1 a	2.97	4.64	4.02	4.44	4.59	5.30	0.37	0.32
B3P86	1	3.1 g	3.03	4.44	4.07	4.33	4.65	5.14	0.34	0.28
B3P86-TDDFT	1	2.7 t	2.89	4.13	3.83	4.15	4.36	5.12	0.40	0.41
B3P86-ADF	2	2.9 a	3.00	4.36	4.07	4.24	4.60	5.04	0.37	0.30
B3LYP	1	2.9 g	3.37	4.42	4.57	4.32	4.98	5.06	0.39	0.28
B3LYP	3	3.9 g	3.33	4.38	4.59	4.12	4.92	4.97	0.43	0.24
B3LYP-TDDFT	1	3.0 t	3.21	3.95	4.46	4.20	4.66	5.11	0.30	0.16
B3LYP-TDDFT	4	2.1 t	3.04	4.12	4.25	4.62	4.48	5.36	0.22	0.28
CASSCF(Roos)	1	1.9 c	4.46	4.07	6.07	4.55	5.61	5.24	0.99	1.03
CASSCF(Roos)	3	4.0 c	4.52	4.08	6.14	4.37	5.61	5.20	1.02	1.06
CASSCF(10,8)	1	2.3 c	4.23	4.00	5.86	4.81	5.33	5.32	0.84	0.77
CASSCF(10,8)	3	3.6 p	4.24	3.99	5.89	4.70	5.31	5.30	0.84	1.30
CASSCF(12,11)	1	3.0 c	4.27	4.08	5.86	4.83	5.61	5.40	0.89	0.94
CASSCF(12,14)	1	5.2 c	4.86	4.22	6.42	4.93	6.01	5.78	1.24	1.43
CASPT2(Roos)	1	2.5 c	3.24	4.15	4.42	4.39	4.84	5.04	0.32	0.22
CASPT2(Roos)	3	4.1 c	3.11	4.06	4.28	4.12	4.68	4.87	0.40	0.23
CASPT2(10,8)	1	2.8 c	3.16	4.15	4.29	4.28	4.81	4.98	0.35	0.24
CASPT2(10,8)	3	4.9 p	2.95	4.06	4.15	3.98	4.84	4.80	0.48	0.38
CASPT2(12,11)	1	3.4 c	3.26	4.15	4.43	4.28	4.81	5.01	0.34	0.19
CASPT2(12,14)	1	5.5 c	3.34	4.19	4.51	4.35	4.93	5.08	0.33	0.25
MRCI(10,8)	1	5.5 p	3.96	4.25	5.40	4.70	5.31	5.38	0.64	0.64
MRCI(10,8)	3	5.7 p	3.97	4.21	5.45	4.52	5.27	5.32	0.65	0.62
MRCI+Q(10,8)	1	5.5 p	3.81	4.33	5.14	4.66	5.27	5.38	0.54	0.54
MRCI+Q(10,8)	3	5.7 p	3.81	4.30	5.18	4.45	5.21	5.31	0.54	0.52
CASPT3(10,8)	1	4.8 p	3.93	4.33	5.32	4.63	5.32	5.43	0.61	0.63
MRDCI[16]	5		3.28	4.00	4.12	4.66	4.84	6.05	0.20	0.20

[a] The basis sets used are 1- cc-pVDZ, 2- ADF #III (polarized double-ζ), 3- aug-cc-pVTZ, 4−3-21G, 5- double-ζ. [b] t is the computer time required on a DEC Au/500 workstation, in s, using (a) ADF, (c) MOLCAS, (g) GAUSSIAN-94, (i) our own INDO-MRCI program, (p) MOLPRO, (t) TURBOMOLE. [c] Estimated as the observed 0−0 line at 3.33 eV plus the average reorganization energy from Table 6. [d] Assignment based on the shown MRDCI results[16] (double-ζ basis). Fischer[17] has suggested that the assignments of T_2 and T_4 may be reversed; T_3 and T_6 may be poorly located.

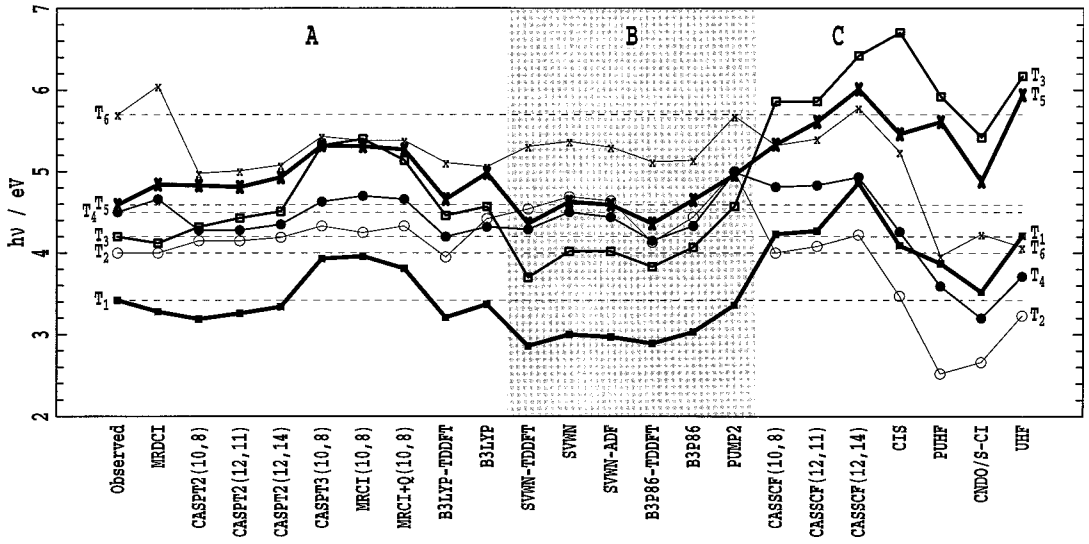

Figure 2. Graphic display of the observed (horizontal dashed lines) and calculated vertical excitation energies for states $T_1 - T_6$, taken from Table 2.

have also been observed within the singlet manifold, and corresponding data for eight valence singlet excited states is given in Table 3 and shown graphically in Figure 3. Of these eight states, seven have firm assignments,[1,6,13,15,16] but a low-lying ^1A_u state remains unobserved. While our names S_n for these states in general follow the assignments of Walker and Palmer[16] and Roos et al.,[6] we list this state as S_3 to avoid confusion as the notation S_2 is widely used[9,10] for $^1B_{2u}$. Recently, equation-of-motion coupled-cluster (EOM-CCSD) and related calculations with triples corrections (EOM-CCSD(T)) calcula-

TABLE 3: Calculated Singlet Vertical Transition Energies, in eV, of Pyrazine at the B3LYP/cc-pVDZ Ground State Geometry Evaluated, except Where Noted, Using the cc-pVDZ Basis, and the RMS Difference from the Assignments of the Observed Energies by Roos et al.[6]

method	$S_1\ ^1B_{3u}$	$S_2\ ^1B_{2u}$	$S_3\ ^1A_u$	$S_4\ ^1B_{2g}$	$S_5\ ^1B_{1g}$	$S_6\ ^1B_{1u}$	$S_7\ ^1B_{1u}$	$S_8\ ^1B_{2u}$	RMS error
observed[16]	3.97[a]	4.81		5.19[b]	6.10	6.51	7.67	7.67	
CIS	5.17	6.12	6.94	6.83	9.42	6.74	8.98	9.25	1.75
CASSCF[c](Roos)	5.24	5.10	6.32	6.28	7.57	8.51	9.65	9.55	1.55
CASSCF(Roos)	5.17	5.02	6.08	6.27	7.41	8.22	10.16	9.61	1.59
CASSCF(10,8)	4.86	5.05	5.92	5.91	7.20	8.56	10.53	10.03	1.72
CASSCF(12,11)	4.98	5.13	5.86	6.23	7.39	8.51	10.23	9.75	1.65
CASSCF(12,14)	5.29	5.26	6.20	6.30	7.37	8.43	11.98	11.37	2.42
CASPT2D[c](Roos)	3.58	4.77	4.37	5.17	6.13	6.68	7.57	7.75	0.13
CASPT2(Roos)	3.88	4.81	4.45	5.51	6.32	6.75	7.71	7.61	0.18
CASPT2[d](10,8)	3.81	4.77	4.33	5.49	6.24	6.61	7.40	7.04	0.29
CASPT2(10,8)	3.83	4.79	4.36	5.50	6.26	6.60	7.43	7.28	0.22
CASPT2(12,11)	3.91	4.75	4.46	5.49	6.26	6.65	7.57	7.41	0.18
CASPT3(10,8)	4.62	5.26	5.33	5.99	6.97	7.17	8.78	8.72	0.84
B3LYP-TDDFT[e]	3.91	5.78	4.35	5.61	6.14	6.95	8.24	8.17	0.52
B3LYP-TDDFT	3.99	5.49	4.59	5.66	6.37	6.58	7.87	7.90	0.35
B3LYP-AVE	3.88	5.11	4.55	5.58	7.01	6.53	7.34	8.62	0.55
B3P86-TDDTF	3.60	5.37	3.97	5.19	5.54	6.48	7.70	7.57	0.31
B3P86-AVE	4.17	5.11	5.01	5.95	7.22	6.54	7.30	8.78	0.70
SVWN-TDDFT	3.47	5.38	3.79	5.06	5.36	6.53	7.71	7.41	0.39
SVWN-AVE	3.48	4.92	4.10	5.19	6.85	5.77	6.49	8.75	0.74
CNDO−S/CI	3.52	4.59	5.98	4.88	7.98	5.98	7.18	7.50	0.79
EOM-CCSD[13]	4.34	5.09	5.20	5.97	7.04	6.96	8.14	7.93	0.56
EOM-CCSD(T)[13]	3.95	4.64	4.81	5.56	6.60	6.58	7.72	7.60	0.25

[a] Estimated as the observed 0−0 line at 3.83 eV plus the average reorganization energy from Table 6. [b] From ref. 80, older works[1] quote 5.5 eV. [c] From Roos et al.[6] at the experimental ground-state geometry using a triple-ζ ANO basis set but ignoring off-diagonal contributions to the CASPT2 energy. [d] Performed using MOLPRO, all other CASPT2 calculations were performed using MOLCAS. [e] 3-21G basis.

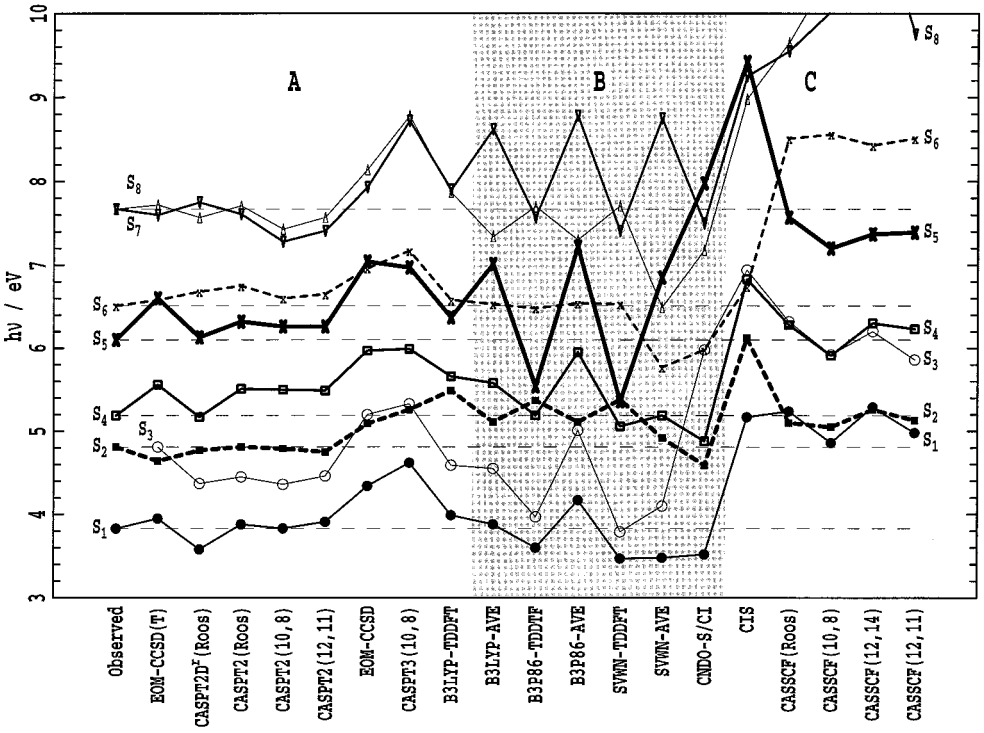

Figure 3. Graphic display of the observed (horizontal dashed lines) and calculated vertical excitation energies for states $S_1 - S_8$, taken from Table 3.

tions have been performed for the singlet states by Del Bene, Watts, and Bartlett,[13] and our notation is consistent with their assignment of the singlet states. The results of their calculations are also shown in Table 3 and Figure 3, along with the results from the CASSCF and CASPT2D calculations of Fülscher, Andersson, and Roos.[6]

Qualitatively, Figure 2 shows that for the triplet states the computational methods can be divided into three categories depending on the major features of the state ordering. Category A contains both the high-quality ab initio methods including the MRDCI method used by Walker and Palmer[16] and the sophisticated B3LYP density functional method. All category C methods fail to correctly assign the lowest energy excited state. In Figure 3 the computational methods are also grouped into three categories depending on their ability to assign the singlet manifold. Most methods attain the same category for both the singlet and triplet states, the exceptions being CIS and CNDO/S-CI which are category B for singlets and C for triplets; category A methods are invariant.

Within the category-A methods, for the singlet states, the

TABLE 4: Dominant Excitations Contributing to the CIS Wavefunctions

state	type	excitation	coefficient
T_1 ($^3B_{3u}$)	(n,π^*)	$20(a_g)\rightarrow 22(b_{3u})$	0.67
T_2 ($^3B_{1u}$)	(π,π^*)	$21(b_{1g})\rightarrow 23(a_u)$	0.53[a]
		$19(b_{2g})\rightarrow 22(b_{3u})$	−0.43
T_3 (^3A_u)	(n,π^*)	$20(a_g)\rightarrow 23(a_u)$	0.69
T_4 ($^3B_{2u}$)	(π,π^*)	$21(b_{1g})\rightarrow 22(b_{3u})$	0.70
T_5 ($^3B_{2g}$)	(n,π^*)	$18(b_{1u})\rightarrow 22(b_{3u})$	0.64
T_6 ($^3B_{1u}$)	(π,π^*)	$21(b_{1g})\rightarrow 23(a_u)$	0.45
		$19(b_{2g})\rightarrow 22(b_{3u})$	0.54[a]

[a] This excitation only is used in the PUMP2, B3LYP, SVWN, SVWN-ADF, and B3P86, and B3P86-ADF calculations.

recent EOM-CCSD(T) results of Del Bene, Watts, and Bartlett[13] are seen to be in excellent qualitative agreement with the CASPT2 and B3LYP-TDDFT results. For the triplet states, in general, the results of the MRDCI calculations of Walker and Palmer[16] are also in good agreement with our CASPT2 and B3LYP results, the only significant difference being that we predict $T_6(^3B_{1u})$ to be 0.6−1.2 eV lower in energy. Their assignment of the shoulder which is somewhat evident in the experimental near-threshold electron-loss spectrum[16] at 5.5−5.9 eV appears to remain sound, however.

Two small differences found within the category A methods for the triplet states are first that B3LYP (but not B3LYP-TDDFT) interchanges the order of the states $T_2(^3B_{1u})$ and $T_4(^3B_{2u})$, and second, the relative ordering of $T_3(^3A_u)$ and $T_4(^3B_{2u})$ is variable. The interchange of T_2 and T_4 is relevant in that Fischer,[17] from an analysis of the vibronic coupling in the $S_0\rightarrow T_1$ absorption, has suggested that the assignments of these two states by Walker and Palmer[16] should be reversed. Indeed, the computational methods grouped in category B in Figure 2 also all show this reversal. These methods include the SVWN and B3P96 density functional approaches as well as the PUMP2 method. They provide a comparable statistical description to the methods in category A for the two states, $T_1(^3B_{3u})$ and $T_5(^3B_{2g})$ for which the experimental assignment is firm, but reorder the intermediate states with $T_3(^3A_u) < T_4(^3B_{2u}) < T_2(^3B_{1u})$. However, for the category B methods, errors exceeding the magnitude of the $T_2 - T_4$ errors are found for $T_1(^3B_{3u})$, and the results for the singlet states are clearly inferior to those from the category A methods.

All of the methods grouped in category C fail to clearly identify the lowest excited state in the manifold, a result of primary importance. In general, all of the methods which do not include dynamic electron correlation comprise this category, although CIS and CNDO/S-CI do fall into category B for the singlet states. Results from the CIS and CNDO/S-CI calculations are especially useful, however, in that they allow the excited states to be described in terms of linear combinations of single-determinant wave functions, and the results are given in Table 4 for the triplet CIS wave functions. There, the excitation is specified in terms of the SCF molecular orbital numbers, symmetries, and σ/π classification. The (π,π^*) states appear as linear combinations of two determinants, as is customary for such transitions in even alternate hydrocarbons. Such mixing is naturally included in the CNDO/S-CI, CIS, CASSCF (etc.), and TDDFT calculations, but for the direct DFT, PUHF, and PUMP2 calculations on the triplet states and the AVE DFT calculations on the singlets, just the major of the two interacting excitations must be selected as detailed in Table 4. It is possible that the switching of the $T_2(^3B_{1u})$ and $T_4(^3B_{2u})$ states by the SVWN, B3P86, and PUMP2 methods arises as the omitted static electron correlation would act to lower T_2 and hence restore the order to that as determined by the category A methods. This seems unlikely, however, as the results obtained using TDDFT, which does include this effect, are not significantly different from those of the direct DFT methods.

TABLE 5: Maximum and RMS Changes of the Calculated Energies of $T_1\rightarrow T_6$ as the Basis Set Is Reduced from aug-cc-pVTZ, in eV

	cc-pVDZ		aug-cc-pVDZ		cc-pVTZ	
method	RMS	max	RMS	max	RMS	max
B3LYP	0.10	0.20	0.02	0.04	0.03	0.06
CIS	0.11	0.26	0.02	0.04	0.04	0.09
CASSCF(Roos)	0.08	0.18				
CASSCF(10,8)	0.05	0.11	0.02	0.04	0.01	0.03
CASPT2(Roos)	0.17	0.27				
CASPT2(10,8)	0.18	0.30			0.09	0.16
MRCI(10,8)	0.08	0.18				
MRCI+Q(10,8)	0.10	0.21				

To aid the quantitative analysis of the calculated vertical excitation energies, in Tables 2 and 3 we report the root-mean-square (RMS) deviations between the calculated and observed transition energies summing over all assigned states. For the triplet manifold is also shown this quantity summed over just the two states $T_1(^3B_{3u})$ and $T_5(^3B_{2g})$ for which the assignment is firm. For the singlet and triplet bands with firm assignments, the methods grouped in category A produce errors ranging up to 0.6 eV while those from category C are typically 1−2 eV.

An important feature is that significant quantitative differences are found between the earlier MRDCI results of Walker and Palmer[16] and our MRCI ones. As our calculations use many more reference determinants, include larger CI, and employ a larger basis set than used in the MRDCI calculations, better results would naively be expected, contrary to observation. Further, while the level of ab initio theory increases from CASPT2D to CASPT2 to CASPT3 to MRCI, it is actually the CASPT2D and CASPT2 results which provide the best agreement with experiment. Clearly, the computed results are very useful in interpreting experimental data, but these ab initio methods do not provide stable, converged excitation energies to within experimental accuracy; much smoother convergence is suggested for EOM-CCSD based methods, however.[13]

The convergence of the calculated energies with respect to the computational level is related to the convergence with respect to both the choice of the active space and the basis set. This connection occurs as, in perturbation theory treatments, it is important to include all strongly coupled states, including basis-set sensitive Rydberg states, in the active space.[24,69] So as to determine the effects of basis-set variation, we have repeated many of the triplet calculations using the larger basis sets aug-cc-pVDZ,[25] cc-pVTZ,[23] and aug-cc-pVTZ.[25] Results for the biggest basis set are given explicitly in Table 2, while the maximum and RMS changes between this and the smaller basis sets are given in Table 5. The maximum and RMS errors associated with the use of the cc-pVDZ basis set are of the order 0.1 and 0.2 eV, respectively, these being somewhat less than the deviations of the calculated numbers from the experimental values. For all methods, the maximum basis-set dependence is found for the (π,π^*) state T_4 $^3B_{2u}$. The aug-cc-pVDZ basis set appears to give results superior to those from the bigger basis set cc-pVTZ, reflecting the well-known[6,16,24,69] importance of the Rydberg states to the valence state energies. Also, the largest basis-set dependence (maximum error 0.3 eV, RMS 0.2 eV) does indeed occur for the perturbative CASPT2 methods, with the active space containing the Rydberg orbitals giving slightly better results than the (10,8) active space. Similar results have been found in more exhaustive studies[24] of the basis-set dependence of CASPT2 energies.

TABLE 6: Excited-State Reorganization Energies λ, in eV

state	exp[a]	PUMP2	SVWN	B3LYP	CIS	CASSCF
S_1 ($^1B_{3u}$)	0.15				0.13	0.15
S_2 ($^1B_{2u}$)	0.19				0.23	0.26
S_3 (^1A_u)					1.08	0.68
T_1 ($^3B_{3u}$)	~0.1	0.09	0.08	0.10	0.10	0.09
T_2 ($^3B_{1u}$)	0.5 ± 0.15	0.62		0.15	0.35	0.37
T_3 (^3A_u)	<0.4	0.65		0.77	1.07	0.72
T_4 ($^3B_{2u}$)	<0.4	0.33		0.25	0.23	0.18
T_5 ($^3B_{2g}$)	0.5 ± 0.25	0.45		0.55	0.49	0.45
T_6 ($^3B_{1u}$)	<0.4			1.25	0.21	0.18

[a] The experimental estimates for the triplet states are made by inspection of the near-threshold electron-loss band contours of Walker and Palmer;[16] that for S_1($^1B_{3u}$) is half of the difference between the observed absorption and fluorescence band maxima in isooctane solution.[22] Note that the observed broadening involves not only contributions from the reorganization energies (λ) but also possible contributions from vibronic coupling. Detailed partitioning of λ into contributions arising from each of the totally symmetric normal modes is reported elsewhere.[21]

The density functional methods produce results comparable with those from the ab initio methods, as has been previously observed[12,35] for approximate DFT calculations on singlet excited states. Here, by studying triplet excited states, we are able to compute the exact transition energy for the density functionals as well and hence determine the effects of the additional DFT approximations. The RMS deviation between the direct and TDDFT energies for the triplet states averaged over all three DFT functionals is quite small, 0.23 eV, this being less than typical deviations with experiment (0.3−0.4 eV). As the TDDFT method does account in some sense for the multideterminant nature of the (π,π*) states, it is not apparent a priori which approach would be expected to give the best results, and the calculations show that they are essentially equivalent in their ability to reproduce the experimental data. Having established the quality of the TDDFT approach through this analysis, we may examine the quality of the averaging approach (AVE) for the singlet states by comparison of the two sets of results. In this case the RMS deviation, averaging over all states and all functionals, is much higher, 0.77 eV. As Table 3 and Figure 3 show, the effects are small for some states and large for others, and the AVE method appears, in general, to be unreliable.

From Table 2 we see that, for the generally applicable and computationally efficient B3LYP-TDDTF method, use of the small 3-21G basis set produces the results which, of all methods considered, show the smallest deviation from experiment for the triplet states. This is a coincidence as this result is not repeated for the singlet manifold (see Table 3), but nevertheless it suggests that this method may be very useful for the determination of the excitation energies of large molecules. Finally, we note, however, that while the tabulated basis-set dependences for B3LYP shown in Table 5 closely parallel those for MRCI+Q and other methods, similar results are not expected if doubly augmented basis sets are used. This is because B3LYP dramatically underestimates the energies of Rydberg states involving 4s or 4p character, consequentially depressing the 3s and 3p Rydberg transitions into the valence region.[73]

IV. Relaxation Energies

The geometries of $S_1 - S_3$, and $T_1 - T_6$ have been optimized using a variety of methods and the results are shown in Table 6 (reorganization energies) and Table 7 (CIS equilibrium geometry changes). Estimated experimental reorganization energies are also provided, these being obtained from inspection of the observed band contours. Realistic experimental estimates are obtained only for the better-resolved states S_1($^1B_{3u}$), S_2($^1B_{2u}$), T_1($^3B_{3u}$), T_2($^3B_{1u}$), and T_5($^3B_{2g}$), and for these the calculated quantities are typically in reasonable agreement with experiment. The exceptions to this are the PUMP2 and direct DFT methods which poorly describe the B_{1u} states, this apparently being due to the explicit treatment of only one of the two key interacting electronic configurations. These notwithstanding, the reorganization energies evaluated using the different methods are in reasonably good agreement with each other.

Concerning the assignment of the experimentally observed bands, the reorganization energy calculations appear to favor the original Walker and Palmer assignment[16] of the contentious states T_2($^3B_{1u}$) and T_4($^3B_{2u}$). However, before reliable conclusions could be drawn, an authoritative deconvolution of the experimental spectra[16] would be required. The situation with regard to T_3(^3A_u) is much clearer. All calculations predict this state to have a very large reorganization energy, of order 0.7−1.0 eV, while the shoulder in the experimental low-energy electron loss spectrum[16] which is attributed to this state is indicative of a much narrower band. It is thus highly unlikely that ^3A_u has been correctly identified; ^1A_u is also unidentified.

The equilibrium geometry changes shown in Table 7 indicate that the A_u states suffer the greatest distortion from the ground-state geometry with the CC bond lengths increasing by 0.123 Å to that of a single CC bond. This result is in accord with the bond orders of the excited states, and it is this displacement which gives rise to the very large reorganization energies shown in Table 5. A curious feature, however, is that T_2($^3B_{1u}$) has similarly lengthened CC bonds but this distortion generates only one-third to one-half of the reorganization energy. To some extent this arises due to the large change in the NCC bond angle in the A_u states, see Table 7; more comprehensively, normal mode analysis[21] shows that this arises because for T_2($^3B_{1u}$) the distortion is entirely in the low-frequency ring deformation mode (CIS $\nu_1 = 985$ cm^{-1}) while for T_3(^3A_u) a similar distortion occurs in this mode but the greatest distortion occurs in the high-frequency ring breathing mode (CIS $\nu_{8a} = 1716$ cm^{-1}).

V. Conclusions

We have investigated the ability of a range of computational methods to predict the vertical excitation and possibly also symmetric relaxation energies for 14 excited electronic states of pyrazine. The most reliable results appear to come from EOM-CCSD(T),[13] CASPT2, and B3LYP methods; B3LYP may reliably be implemented either directly (for triplet states only) or approximately, using TDDFT, but heuristic state-averaging (AVE) assumptions are unreliable. For the CASSCF-based methods, the calculated energies vary significantly with the choice of the active space and basis set, but all post-CASSCF methods suggest similar assignments and appear qualitatively robust. Numerically, the most accurate results come from application of the methodological, active-space, and basis-set combinations determined by Roos et al.,[6] but the CASPT2D results do change considerably on improvement of the methodology to CASPT2, CASPT3, or MRCI, and the CASPT2 results are somewhat active-space and basis-set dependent. Alternatively, EOM-CCSD(T) appears to provide a systematic improvement on EOM-CCSD, and these ab initio time-dependent methods may prove to be more robust that the ab initio CASSCF-based methods. However, CASSCF-based methods will always be more appropriate for molecules whose ground state is not properly described in terms of a single-determinant wave function. This issue is explored elsewhere[73,74] where we

TABLE 7: Calculated D_{2h}-Optimized Equilibrium Geometries for Various Electronic States[a]

	S_0 (^1A_g)											
	exp[b]	B3LYP	SCF	S_1 ($^1B_{3u}$)	S_2 ($^1B_{2u}$)	S_3 (^1A_u)	T_1 ($^3B_{3u}$)	T_2 ($^3B_{1u}$)	T_3 (^3A_u)	T_4 ($^3B_{2u}$)	T_5 ($^3B_{2g}$)	T_6 ($^3B_{1u}$)
CN	1.337	1.339	1.320	0.013	0.012	−0.041	0.016	0.001	−0.041	0.024	0.047	0.038
CC	1.400	1.399	1.389	0.000	0.000	.123	−0.004	0.109	0.123	0.031	−0.038	0.016
CH	1.096	1.095	1.083	−0.002	−0.002	−0.003	−0.003	−0.002	−0.004	0.001	−0.004	−0.003
NCC	122	122	122	−2	−2	−6	−1	0	−6	3	−4	1
CCH	117	121	121	−2	−2	−1	−1	−1	−1	−3	4	0

[a] Absolute bond lengths and angles are given for S_0, but for the excited states changes from the SCF ground-state values are given. Bond lengths are in Å, bond angles in degrees; CIS geometries are shown for excited states, and the cc-pVDZ is used throughout. Optimized Cartesian coordinates for these states obtained using all computational methods are provided elsewhere;[21] see also, e.g., refs 11,16. [b] Electron diffraction.[81]

consider the applicability of EOM-CCSD and TDDFT to excited states involving either significant bond extension or bond breakage.

For the triplet states of pyrazine, the identity of at least three observed states remains uncertain. The (apparently) most reliable theoretical methods all list $^3B_{2u}$ and $^3B_{1u}$ in the order given originally by Walker and Palmer,[16] but the energy differences between the states (observed 0.5 ± 0.1 eV) is less than the absolute accuracy of the methods (for which typical RMS errors are 0.2−0.3 eV per state while maximum errors are ca. 0.5 eV). Reorganization energy calculations also tentatively support this assignment. Nevertheless, the empirical vibronic coupling calculations of Fischer,[17] which analyze the vibrational structure of $T_1(^3B_{3u})$, do suggest that the assignment of these states should be reversed, and we feel that the theoretical calculations are not sufficiently reliable to authoritatively preclude this. To further resolve this issue, elsewhere[21] we calculate a priori the vibrational structure of this electronic state.

Other key unresolved issues concern the location of $S_3(^1A_u)$ and $T_3(^3A_u)$, the explanation of the possible chaos in the $S_0 \rightarrow T_1$ absorption spectrum of pyrazine crystal[75] at 0.2 eV above the band origin, and the explanation of the observed very rapid vibrational relaxation of T_1.[76] A possible interpretation of the unexplained experimental results is that the origin of an electronic state lies between those of $T_1(^1B_{3u})$ and $S_1(^1B_{3u})$. Most discussion of this possibility has focused on the feasibility of the location of either $T_2(^3B_{1u})$ or $T_4(^3B_{2u})$ in this region, but the failure of phosphorescence excitation[77] or low-energy electron-loss[16] spectra to detect these states in this region indicates that they are not located there.

It may be possible that the observed spectral features can be interpreted solely in terms of the properties of the T_1 state (see, e.g., Heller et al.[78] for possible mechanisms). If, however, an additional state is located between T_1 and S_1, then our calculations suggest that the most likely candidate is $T_3(^3A_u)$. Vertically, the most reliably computational methods place T_3 ca. 0.2 eV above $T_2(^3B_{1u})$ with S_3 either slightly above or slightly below $S_2(^1B_{2u})$, and Table 6 indicates that on relaxation the energies of these states decrease significantly. To further explore this, we show in Table 8 the CASPT2(10,8) and B3LYP-TDDFT energy differences for nine excited states evaluated at the CIS geometries individually optimized in D_{2h} symmetry. In this table, the states are listed in terms of their CASPT2 relative energy: both $T_3(^3A_u)$ and $S_3(^1A_u)$ are predicted to lie between T_1 and S_1 by both computational methods. Interestingly, $T_2(^3B_{1u})$, which has a higher reorganization energy than S_1, is predicted to be of equal energy with S_1 by CASPT2 and to fall below T_3 and S_3 by B3LYP-TDDFT. The arguments which support the assignment of T_3 as the proposed state between T_1 and S_1 are: (1) T_3 has a large reorganization energy and hence its low-energy electron-loss spectrum[16] would be very broad with a maximum in the vicinity of a number of sharp features. Hence, its lack of observation in this experiment can be understood. (2) This state is dark to direct observation by absorption/emission spectroscopic methods, and hence its lack of observation in phosphorescence excitation spectra[77] can be understood. (3) The potential energy minimum of this state lies geometrically distant from the Franck−Condon region. Hence, direct vibronic interactions of it with T_1 would be minimized by the necessarily small overlap of the vibrational wave functions. (4) T_3 is an (n,π^*) state whose symmetry may be lowered from D_{2h}. In fact, B3LYP calculations[21] predict that its energy is lowered by distortions in both ν_{8b} (from vibronic coupling to T_1) and ν_{10a} (from vibronic coupling to T_2), while CASSCF predicts energy lowering on distortion in ν_{12}. Such symmetry lowering would impart a permanent dipole moment to the electronic state, making the transition intensity solvent sensitive, as is implied by the experimental data, and enhancing vibrational energy transfer processes, as evidenced by the crystal phosphorescence and vibrational relaxation experiments.

TABLE 8: Calculated Adiabatic Excitation Energies, in eV, Evaluated at D_{2h}-Optimized SCF (Ground State) and CIS (Excited State) Geometries

state	obsd[16]	CASPT2(10,8)	B3LYP-TDDFT
T_1 ($^3B_{3u}$)	3.33	3.07	3.10
T_3 (^3A_u)		3.62	3.73
S_3 (^1A_u)		3.67	3.86
S_1 ($^1B_{3u}$)	3.83	3.70	3.87
T_2 ($^3B_{1u}$)		3.71	3.49
T_4 ($^3B_{2u}$)		3.97	3.99
T_5 ($^3B_{2g}$)		4.32	4.16
S_2 ($^1B_{2u}$)		4.49	5.28
T_6 ($^3B_{1u}$)		4.68	4.90

One feature of the calculated results is not so readily interpretable, however, and this is the simultaneous location of $S_3(^1A_u)$ within the T_1-S_1 gap. All calculations indicate that the singlet−triplet splitting between the A_u states is less than 0.1 eV and so if T_3 were to be located adiabatically 0.2 eV above T_1 then S_3 must be also located below S_1. One would expect some manifestation of this to have been observed, if indeed it is the case, but perhaps it does lie there but has not been detected due to its small vibrational overlap with S_1.

In the choice of an appropriate computational method for a particular problem, the required amount of computer time (and other resources) is often critical. For the 33 methods used to determine triplet-state energies, the required computer time is indicated in Table 2. These times range over 7 orders of magnitude, from CNDO/S-CI to MRCI. While the CNDO/S-CI results are clearly inferior to many of the more expensive methods, they are useful (particularly for the singlet states) and, for sufficiently large molecules, this remains the only currently feasible technique, though possible alternative techniques are being developed.[79] The DFT-based methods have the advantage that their cost increases at the lowest rate with increasing molecular size. Particularly, B3LYP appears the method of choice for quality calculations on medium-sized systems.

Acknowledgment. P.W. is indebted to the Swiss National Science Foundation for support, while J.R.R. is indebted to the Australian Research Council. We thank Dr. George Bacskay from the University of Sydney for helpful discussions.

References and Notes

(1) Innes, K. K.; Ross, I. G.; Moomaw, W. R. *J. Mol. Spectrosc.* **1988**, *132*, 492.

(2) Del Bene, J. E. *J. Am. Chem. Soc.* **1975**, *112*, 9405.

(3) Del Bene, J. E. *Chem. Phys.* **1976**, *15*, 463.

(4) Wadt, W. R.; Goddard, W. A., III *J. Am. Chem. Soc.* **1975**, *97*, 2034.

(5) Wadt, W. R.; Goddard, W. A., III; Dunning, T. H. *J. Chem. Phys.* **1976**, *65*, 438.

(6) Fülscher, M. P.; Andersson, K.; Roos, B. O. *J. Phys. Chem.* **1992**, *96*, 9204.

(7) Foresman, J. B.; Head-Gordon, M.; Pople, J. A.; Frisch, M. J. *J. Phys. Chem.* **1992**, *96*, 135.

(8) Ågren, H.; Knuts, S.; Mikkelsen, K. V.; Jensen, H. J. Aa. *Chem. Phys.* **1992**, *159*, 211.

(9) Woywod, C.; Domcke, W.; Sobolewski, A. L.; Werner, H.-J. *J. Chem. Phys.* **1994**, *100*, 1400.

(10) Stock, G.; Woywod, C.; Domcke, W.; Swinney, T.; Hudson, B. C. *J. Chem. Phys.* **1995**, *100*, 1.

(11) Martin, J. M. L.; Van Alsenoy, C. *J. Phys. Chem.* **1996**, *100*, 6973.

(12) Bauernschmitt, R.; Ahlrichs, R. *Chem. Phys. Lett.* **1996**, *256*, 454.

(13) Del Bene, J. E.; Watts, J. D.; Bartlett, R. J. *J. Chem. Phys.* **1997**, *106*, 6051.

(14) Fischer, G. *Vibronic coupling: The interaction between the electronic and nuclear motions*; Academic Press: London, 1984.

(15) Bolovinos, A.; Tsekeris, P.; Philis, J.; Phantos, E.; Andritsopoulos, G. *J. Mol. Spectrosc.* **1984**, *103*, 240.

(16) Walker, I. C.; Palmer, M. H. *Chem. Phys.* **1991**, *153*, 169.

(17) Fischer, G. *Can. J. Chem.* **1993**, *71*, 1537.

(18) Merchán, M.; Ortí, E.; Roos, B. O. *Chem. Phys. Lett.* **1994**, *226*, 27.

(19) Del Bene, J.; Jaffe, H. H. *J. Chem. Phys.* **1968**, *48*, 1807, 4050.

(20) Ellis, R. L.; Kuehnlenz, G.; Jaffé, H. H. *Theor. Chim. Acta* **1972**, *26*, 131.

(21) Weber, P.; Reimers, J. R. *J. Phys. Chem.*, accepted for publication.

(22) Baba, H.; Goodman, L.; Valenti, P. C. *J. Am. Chem. Soc.* **1966**, *88*, 5410.

(23) The atoms boron through neon and hydrogen, Dunning, T. H., Jr. *J. Chem. Phys* **1989**, *90*, 1007.

(24) Fülscher, M. P.; Roos, B. O. *Theor. Chim. Acta* **1994**, *87*, 403.

(25) Dunning, T. H., Jr.; Harrison, R. J. *J. Chem. Phys* **1992**, *96*, 6796.

(26) Slater, J. C. *Quantum theory of molecules and solids. Vol. 4: The self-consistent field for molecules and solids*; McGraw-Hill: New York, 1974.

(27) Vosko, S. H.; Wilk, L.; Nusair, M. *Can. J. Phys.* **1980**, *58*, 1200.

(28) Perdew, J. P. *Phys. Rev. B* **1986**, *33*, 8822.

(29) Becke, A. D. *J. Chem. Phys.* **1993**, *98*, 5648.

(30) Gunnarsson, O.; Lundqvist, B. I. *Phys. Rev. B* **1976**, *13*, 4274.

(31) Frisch, M. J.; Trucks, G. W.; Schlegel, H. B.; Gill, P. M. W.; Johnson, B. G.; Robb, M. A.; Cheeseman, J. R.; Kieth, T. A.; Petersson, G. A.; Montgomery, J. A.; Raghavachari, K.; Al-Laham, M. A.; Zakrzewski, V. G.; Ortiz, J. V.; Foresman, J. B.; Cioslowski, J.; Stefanov, B. B.; Nanayakkara, A.; Challacombe, M.; Peng, C. Y.; Ayala, P. A.; Chen, W.; Wong, M. W.; Andres, J. L.; Replogle, E. S.; Gomperts, R.; Martin, R. L.; Fox, D. J.; Binkley, J. S.; DeFrees, D. J.; Baker, J.; Stewart, J. J. P.; Head-Gordon, M.; Gonzalez, C.; Pople, J. A. *Gaussian 94*; Gaussian Inc.: Pittsburgh, 1995.

(32) te Velde, G.; Baerends, E. J. *J. Comput. Phys.* **1992**, *99* ADF 2.3.0, Theoretical Chemistry, Vrije Universiteit, Amsterdam.

(33) Bacskay, G. B.; Reimers, J. R.; Nordholm, S. *J. Chem. Educ.* **1997**, *74*, 1494.

(34) Ziegler, T.; Rauk, A.; Baerends, B. J. *Theor. Chim. Acta* **1977**, *43*, 261.

(35) Cramer, C. J.; Dulles, F. J.; Giesen, D. J.; Almlöf, J. *Chem. Phys. Lett.* **1995**, *245*, 165.

(36) Hu, C.-H.; Chong, D. P. *Chem. Phys. Lett.* **1996**, *262*, 719.

(37) Frank, I.; Hutter, J.; Marx, D.; Parrinello, M. *J. Chem. Phys.* **1998**, *108*, 4060.

(38) von Barth, U. *Phys. Rev. A* **1979**, *20*, 163.

(39) Daul, C.; Baerends, E. J.; Vernooijs, P. *Inorg. Chem.* **1994**, *33*, 3538.

(40) Hass, K. C.; Schneider, W. F.; Estévez, C. M.; Bach, R. D. *Chem. Phys. Lett.* **1996**, *263*, 414.

(41) Gross, E. K. U.; Olivera, L. N.; Kohn, W. *Phys. Rev. A* **1988**, *37*, 2805.

(42) Kryachko, E. S.; Ludena, E. V. *Energy density functional theory of many-electron systems*; Kluwer: Dordrecht, 1990.

(43) Koga, T. *J. Chem. Phys.* **1991**, *95*, 4306.

(44) Warken, M. *J. Chem. Phys.* **1995**, *103*, 5554.

(45) Gardet, G.; Rogemond, F.; Chermette, H. *Theor. Chim. Acta* **1995**, *91*, 249.

(46) Nagy, A. *J. Phys. B* **1996**, *29*, 389.

(47) Nagy, A. *Int. J. Quantum Chem.* **1998**, *98*, 681.

(48) Filippi, C.; Umrigar, C. J.; Gonze, X. *J. Chem. Phys.* **1997**, *107*, 9994.

(49) Görling, A. *Phys. Rev. A* **1996**, *54*, 3912.

(50) Savin, A.; Umrigar, C. J.; Gonze, X. In *Electronic density functional theory: recent progress and new directions*; Dobson, J. F., Vignale, G., Das, M. P., Eds.; Plenum: New York, 1997.

(51) Stückl, A. C.; Daul, C. A.; Güdel, H. U. *Int. J. Quantum Chem.* **1997**, *61*, 579.

(52) Chattaraj, P. K.; Ghosh, S. K.; Liu, S.; Parr, R. G. *Int. J. Quantum Chem.* **1996**, *60*, 535.

(53) Parusel, A. B. J.; Köhler, G.; Grimme, S. *J. Phys. Chem. A* **1998**, *102*, 6297.

(54) Liu, W.; Dolg, M.; Li, L. *J. Chem. Phys.* **1998**, *108*, 2886.

(55) Fronzoni, G.; Stener, M.; Decleva, P.; De Alti, G. *Chem. Phys.* **1998**, *232*, 9.

(56) Bauernschmitt, R.; Häser, M.; Treutler, O.; Ahlrichs, R. *Chem. Phys. Lett.* **1997**, *264*, 573.

(57) Wiberg, K. W.; Stratman, R. E.; Frisch, M. J. *Chem. Phys. Lett.* **1998**, *297*, 60.

(58) Stratman, R. E.; Scuseria, G. E.; Frisch, M. J. *J. Chem. Phys.* **1998**, *109*, 8219.

(59) van Gisbergen, S. J. A.; Kootstra, F.; Schipper, P. R. T.; Gritsenko, O. V.; Snijders, J. G.; Baerends, E. J. *Phys. Rev. A* **1998**, *57*, 2556.

(60) Ahlrichs, R.; Bär, M.; Baron, H.-P.; Bauernschmitt, R.; Böcker, S.; Ehrig, M.; Eichkorn, K.; Elliot, S.; Haase, F.; Häser, M.; Horn, H.; Huber, C.; Huniar, U.; Kattannek, M.; Kölmel, C.; Kollwitz, M.; Ochsenfeld, C.; Öhm, H.; Schäfer, A.; Schneider, U.; Treutler, O.; von Arnim, M.; Weigend, F.; Weis, P.; Weiss, H. *TURBOMOLE*; Quantum Chemistry Group: University of Karlsruhe, 1997: Version 4.

(61) Foresman, J. B.; Head-Gordon, M.; Pople, J. A.; Frisch, M. J. *J. Phys. Chem.* **1992**, *96*, 135.

(62) Andersson, K.; Blomberg, M. R. A.; Füscher, M. P.; Karlström, G.; Lindh, R.; Malmqvist, P. -Å.; Neogrády, P.; Olsen, J.; Roos, B. O.; Sadlej, A. J.; Seijo, L.; Serrano-Andrés, L.; Siegbahn, P. E. M.; Widmark, P.-O. MOLCAS; University of Lund: Sweden, Version 4.

(63) Andersson, K.; Malmqvist, P. -Å.; Roos, B. O. *J. Chem. Phys.* **1992**, *96*, 1218.

(64) Werner, H.-J.; Knowles, P. J.; Almlöf, J.; Amos, R. D.; Deegan, M. J. O.; Elbert, S. T.; Hampel, C.; Meyer, W.; Peterson, K.; Pitzer, R.; Stone, A. J.; Taylor, P. R.; Lindh, R.; Mura, M. E.; Thorsteinsson, T. MOLPRO-97 program package.

(65) Werner, H. J. *Mol. Phys.* **1996**, *89*, 645.

(66) Werner, H.-J.; Knowles, P. J. *J. Chem. Phys.* **1988**, *89*, 5803.

(67) Knowles, P. J.; Werner, H.-J. *Chem. Phys. Lett.* **1988**, *145*, 514.

(68) Davidson, E. R. *Int. J. Quantum Chem.* **1974**, *8*, 61.

(69) Roos, B. O.; Andersson, K.; Fülscher, M. P. *Phys. Chem. Lett.* **1992**, *192*, 5.

(70) Crossley, M. J.; Johnston, L. A.; Reimers, J. R.; Hush, N. S. *J. Am. Chem. Soc.* **1999**, in preparation.

(71) Reimers, J. R.; Hall, L. E.; Crossley, M. J.; Hush, N. S. *J. Phys. Chem. A* **1999**, *103*, 4385.

(72) Zeng, J.; Hush, N. S.; Reimers, J. R. *J. Phys. Chem.* **1996**, *100*, 9561.

(73) Cai, Z.-L.; Reimers, J. R. *J. Chem. Phys.*, submitted.

(74) Cai, Z.-L.; Reimers, J. R. *J. Chem. Phys.*, in press.

(75) Hochstrasser, R. M.; Marzzacco, C. *J. Chem. Phys.* **1968**, *49*, 971.

(76) Wu, F.; Weisman, B. *J. Chem. Phys.* **1999**, *110*, 5047.

(77) Tomer, J. L.; Holtzclaw, K. W.; Pratt, D. W.; Spangler, L. H. *J. Chem. Phys.* **1988**, *88*, 1528.

(78) Heller, E. J.; Stechel, E. B.; Davis, M. J. *J. Chem. Phys.* **1980**, *73*, 4720.

(79) Froese, R. D. J.; Morokuma, K. *Chem. Phys. Lett.* **1996**, *263*, 393.

(80) Okuzawa, Y.; Fufii, M.; Ito, M. *Chem. Phys. Lett.* **1990**, *171*, 341.

(81) Bormans, B. J. M.; De With, G.; Mijhoff, F. C. *J. Mol. Struct.* **1977**, *42*, 121.